Characterization of the I(|Ω|=1)–X^{1}Σ^{+}(0,0) band of thorium oxide

Damian L. Kokkin, Timothy C. Steimle, and David DeMille

Phys. Rev. A **91**, 042508 — Published 27 April 2015

DOI: 10.1103/PhysRevA.91.042508

Characterization of the $I(|\Omega| = 1) - X\,^1\Sigma^+(0,0)$ Band of Thorium Oxide, ThO

Damian L. Kokkin and Timothy C. Steimle
Department of Chemistry and Biochemistry
Arizona State University
Tempe, AZ 85287-1604

David DeMille
Department of Physics
Yale University
PO Box 208120
New Haven, CT 06520

Last Modified: April 9, 2015

Send Proofs to: Prof. T. C. Steimle, Department of Chemistry and Biochemistry, Arizona State University, Tempe, Arizona 85287-1604

- e-Mail: Tsteimle@ASU.edu

Abstract

The $I(|\Omega|=1)-X^1\Sigma^+(0,0)$ band near 512 nm of thorium oxide, ThO, has been recorded and analyzed field-free and in the presence of both static electric and magnetic fields. The determined T_{00}, B, and q field-free parameters for the $I(|\Omega|=1)(v=0)$ state are (in cm^{-1}) 19539.3823±0.0003, 0.32869 ± 0.00003, and 0.00154 ± 0.00005. The Zeeman-induced shifts and splittings of the low-J lines were analyzed to determine g-factors and suggest that the $I(|\Omega|=1)(v=0)$ state has a dominant $^1\Pi$ character. The Stark tuning of the low-J lines was analyzed to determine the permanent electric dipole moment, μ_{el}, for the $I(|\Omega|=1)(v=0)$ state of 4.25 ± 0.02 D.

I. INTRODUCTION

The current upper limit for the magnitude of the electron electric dipole moment (eEDM), $|d_e|$, is 8.7×10^{-29} e·cm and has been determined in an experiment involving the static electric and magnetic field induced effects on the J=1 rotational level of the $H^3\Delta_1(v=0)$ state of thorium oxide, ThO [1]. Recently, we reported on the visible and near ultraviolet excitation spectrum of ThO recorded at medium resolution and the subsequent dispersed fluorescence and radiative lifetimes [2]. Based upon those observations, a possible new optical pumping and detection scheme for the eEDM measurements was proposed. This scheme involves excitation of the $H^3\Delta_1 \rightarrow I(|\Omega|=1)$ (0,0) band and detecting the subsequent $I(|\Omega|=1)$ - $X^1\Sigma^+$ (0,0) fluorescence. Here we report on the first high-resolution spectroscopic study of the $I(|\Omega|=1)-X^1\Sigma^+(0,0)$ band

and determination of the fine structure parameters, the permanent electric dipole moments, μ_{el}, and the magnetic g-factors for the $I(|\Omega|=1)(v=0)$ state.

There are no previous reports of high-resolution laser spectroscopic measurements of the $I(|\Omega|=1)-X^1\Sigma^+(0,0)$ band. The high temperature emission spectrum of the $I(|\Omega|=1)-X^1\Sigma^+(0,0)$ band has been recorded and rotationally analyzed [3]. The spectrum under these conditions is highly congested and overlapped with the low-rotational features not assigned. Strong, local, perturbations of both parity levels at high-J (>50) were noted. The $I(|\Omega|=1)$ state was assigned as a Hund's case (a) $^1\Pi_1$ state and the perturbing state as the $G^1\Delta_2$ state. The $X^1\Sigma^+(v=0)$ state is well characterized by microwave spectroscopy [4]. In addition, the permanent electric dipole moment, μ_{el}, for the $X^1\Sigma^+(v=0)$ states has been determined from the analysis of the optical Stark spectroscopy of the $E(\Omega=0^+) - X^1\Sigma^+$ (1,0) band [5]. The experimentally determined value for the $X^1\Sigma^+(v=0)$ state of 2.782 ±0.012 D was close to the most recent theoretical predicted value 2.93 D [6] .

Properties of the numerous low-lying excited states arising from the $Th^{+2}(7s^16d^1)O^{-2}(2p^6)$ configuration and the $^3\Sigma^-$ and $^3\Phi$ states arising from the $Th^{+2}(6d^2)O^{-2}(2p^6)$ configurations [7, 8] have been predicted. Although the term values for some of predicted states are in the correct energy range, none were assigned as the $I(|\Omega|=1)$ state. Based on ligand field theory, the $I(|\Omega|=1)$ state has the formal electronic configuration $Th^{2+}(7s5f)O^{2-}$ [9].

II. EXPERIMENT

The experimental set up used in the present study is similar to that used in the previous study of the $E(\Omega=0^+) - X^1\Sigma^+$ (1,0) band [5]. A supersonic molecular beam sample was probed by the output of a single frequency cw-dye laser and the resulting laser induced fluorescence (LIF) was monitored on resonance through a ±10 nm band pass filter centered at 510 nm. Spectral line widths of less than 40 MHz full width at half maximum were achieved by a combination of molecular beam collimation and relatively low laser intensity(< 50 mW, unfocused). For the Stark measurements, static electric fields were generated by application of a voltage across a pair of highly transmitting, conducting, neutral density filters straddling the region of molecular fluorescence. The field strength was calibrated by means of a voltmeter and mechanical measurement of the Stark plate spacing. The systematic errors due to the electric field strength calibration were estimated to be less than 2%. Zeeman spectra were recorded using field strengths of 3163 gauss, which were generated by rare earth magnets attached to an iron yoke. The molecular beam passed through 5.0 mm holes in the center of the magnet/yoke assembly. The magnetic field was measured by recording the optical Zeeman effect of ^1S-$^3P_1$ transition of atomic calcium [10]. The systematic errors due to the magnetic field calibration were estimated to be less than 1%. A polarization rotator was used to align the electric field vector of the linearly polarized laser radiation either parallel ″||″ or perpendicular ″⊥″ to that of the applied electric or magnetic field or electric field vector.

The absolute wavenumbers were measured by recording the I_2 *B*-*X* system at sub-Doppler resolution [11]. Extrapolation from the highest wavenumber region of the I_2 calibration spectrum near 19,200 cm^{-1} to the $I(|\Omega|=1) - X\,^1\Sigma^+(0,0)$ band, which is near

19,530 cm^{-1}, was performed by monitoring the transmission of an actively stabilized and calibrated confocal etalon. The same stabilized etalon was used to measure the Stark and Zeeman induced shifts.

III. OBSERVATION

The field-free laser excitation spectrum near the origin of the $I(|\Omega| = 1) - X\,^1\Sigma^+(0,0)$ band is presented in Figure 1 where the expected *P*, *Q*, and *R*-branch structure is readily identified. The spectrum is a collection of numerous 7 GHz wide scans and is not corrected for variation in molecular production and/or laser power. The LIF signals of twenty ablation pulses at each laser wavelength were co-added to enhance the signal to noise. The individual lines have a full width at half maximum of approximately 30 MHz. The measured field-free transition wavenumbers, assignment and the difference between the observed and predicted wavenumbers for twenty branch features are given in Table I.

The *P*(2), *Q*(1), and *R*(0) lines were selected for optical Stark measurements. The *R*(0) (19 539.7127 cm^{-1}) line recorded field free and in the presence of 278 V/cm static electric field with perpendicular polarization ($\Delta M_J = \pm 1$) is presented in Figure 2, along with the associated energy levels. The field-free line rapidly splits into two features due to the small Ω-doubling of the *J*=1 levels of the $I(|\Omega| = 1)$ state**.** The weaker, lower frequency feature is the electric field induced transition to the lower energy parity component which is absent in the field free spectrum. The 48 measured Stark shifts, differences between observed and calculated shifts, and the quantum number assignments are given in Table II.

The $R(0)$, $Q(1)$, $Q(2)$, and $P(2)$ lines were selected for optical Zeeman measurements. The $R(0)$ and $Q(1)$ lines recorded field-free and in the presence of a 3163 Gauss field with nominal perpendicular polarization ($\Delta M_J = \pm 1$) are present in the upper and lower panels of Figure 3, respectively. The fourteen measured Zeeman shifts and corresponding seven splittings between spectral features having common $|M_J|$ are given in Table III. Also presented are the differences between observed and calculated splittings and the quantum number assignments.

V. ANALYSIS

The field-free energies for the $X^1\Sigma^+$ (v=0) state were modeled using the simple formula:

$$E(X\,^1\Sigma^+) = BJ(J+1). \qquad (1)$$

The rotational constant, B, was constrained to the previously determined value of 0.331967 cm^{-1} [5]. The energy levels of the $I(|\Omega| = 1)$ state were modelled using an effective Hamiltonian appropriate for a $^1\Pi$ state:

$$\hat{H}^{eff} = B\hat{R}^2 - D\hat{R}^4 + q(e^{-2i\phi}\hat{J}_+\hat{S}_- + e^{2i\phi}\hat{J}_-\hat{S}_+) \qquad (2)$$

where $\hat{\mathbf{R}}$ is the rotational operator, $\hat{J}_\pm$ and $\hat{S}_\pm$ are the shift operators of the total angular momentum, **J** and the total electron spin angular momentum, **S**. The azimuthal coordinate of the electrons is ϕ. The field-free energies for the state were obtained by constructing and diagonalizing a 2×2 matrix representation using Hund's case (*a*) basis. The 20 precisely measured field-free transition wavenumbers of Table I were used in a least squares fit to produce optimized rotational, B, Λ-doubling, q, and band origin, T_{00} constants for the $I(|\Omega| = 1)$ state. The centrifugal distortion correction parameters for the

ground and excited states, D, were set to zero, indicating that the change in his parameter upon excitation is negligible. The optimized values for T_{00}, B, and q are (in cm^{-1}) 19539.3823±0.0003, 0.32869±0.00003 and 0.00154±0.00005 respectively. The standard deviation of the fit is 0.0005 cm^{-1}, which is commensurate with the estimated measurement uncertainty. Under the assumption that the determined effective rotational constant B does not have a major contribution from higher order effects, the internuclear separation of the $I(|\Omega| = 1)$ state is 1.8514±0.0002Å.

The interaction between the static electric field, $\vec{E}$, and the molecular electric dipole moment, $\vec{\mu}_{el}$, was treated using the standard Stark Hamiltonian:

$$\hat{H}^{Stark} = -\vec{\mu}_{el} \cdot \vec{E} . \qquad (3)$$

The predicted Stark shifts in the $X^1\Sigma^+(v=0)$ state were obtained by diagonalization of a 4×4 matrix representation constructed using the Hund's case (a) basis set for $J'' = 0$-3. Similarly, the predicted Stark shifts in the $I(|\Omega| = 1)(v = 0)$ state were obtained by diagonalization of an 8×8 matrix representation constructed using the Hund's case (a) basis set for $J' = 1$-4. The observed Stark shifts of Table II were analyzed using a non-linear least squares fitting program. The $|\vec{\mu}_{el}|$ for the $X^1\Sigma^+(v=0)$ state was constrained to the previously determined value of 2.782 D [5]. The resulting optimized $|\vec{\mu}_{el}|$ value for the $I(|\Omega| = 1)(v = 0)$ state is 4.25 ± 0.02D. The error limits represent a 90% statistical confidence level.

As expected, there was no evidence of magnetic field induced shifts of the $X^1\Sigma^+(v=0)$ state energy levels. There was also no evidence of parity dependence to the splittings.

The splitting between the spectral features having common $|M_J|$ values was modelled, rather than the shift of individual components, because this splitting could be measured more accurately. The splittings, $\Delta\nu$, were fit to the expression:

$$\Delta\nu = 2g_J^{eff}\mu_B|M_J|\vec{B}. \quad (4)$$

The determined g_J^{eff} values for $J'=1$ and 2 are 0.5260±0.0006 and 0.1688±0.004, respectively. The error for the $J'=1$ level is significantly smaller than that for the $J'=2$ because of the much larger data set.

V. DISCUSSION

The determined T_{00}, B, and q constants for the $I(|\Omega|=1)(v=0)$ state from the analysis of the low-J branch features performed here are not directly comparable with the previously determined values [3] obtained from the analysis of the perturbed, high-J, branch features. Unlike the previous study, the low-J branch features of the $I(|\Omega|=1)-X^1\Sigma^+(0,0)$ band have been successfully modeled assuming that the $I(|\Omega|=1)(v=0)$ state is an unperturbed $^1\Pi$ state. The determined $|\vec{\mu}_{el}|$ for the $I(|\Omega|=1)(v=0)$ state of 4.25 ± 0.02D is significantly larger than the 2.782±0.012 D and 3.534±0.010 D values for the $X^1\Sigma^+(v=0)$ and $E(\Omega=0^+)(v=1)$ states, respectively. The observed ordering of $|\vec{\mu}_{el}|(X^1\Sigma^+) < |\vec{\mu}_{el}|(E(\Omega=0^+)) < |\vec{\mu}_{el}|(I(|\Omega|=1))$ is consistent with the ligand field theory prediction [9] that the dominant configurations for the $X^1\Sigma^+$, $E(\Omega=0^+)$, and $I(|\Omega|=1)$ states are $Th^{2+}(7s^2)O^{2-}$, $Th^{2+}(7s6d)O^{2-}$ and $Th^{2+}(7s5f)O^{2-}$, respectively. The $E(\Omega=0^+)$ and $I(|\Omega|=1)$ state differ from the $X^1\Sigma^+$ state by the

promotion of an electron in a highly polarizable 7*s* orbital to a less polarizable 6*d* or 5*f* orbital, respectively.

In addition to being useful for predicting the magnetic tuning, the determined g_J^{eff} values provide valuable insight into the nature of the $I(|\Omega|=1)(v=0)$ state. The Hund's case (a) expectation value for the electronic orbital and electronic spin contribution to the Zeeman operator is:

$$\left\langle J\Omega M_J \left| \left\langle S\Sigma \left| \left\langle n\Lambda \right| -\vec{\mu}_m \cdot \vec{B} \left| n\Lambda \right\rangle \right| S\Sigma \right\rangle \right| J\Omega M_J \right\rangle = g_J^{eff} \mu_B B M_J , \quad (6)$$

where

$$g_J^{eff} \equiv \left[g_L \Lambda + g_S \Sigma \right] / \left[J(J+1) \right] . \quad (7)$$

The g_J^{eff} values for the *J*=1 (or *J*=2) rotational levels of a Hund's case (a) $^3\Sigma_1^{\pm}$, $^3\Delta_1$, $^3\Pi_1$, and $^1\Pi_1$ states are approximately 1.00, 0.00, 0.50, and 0.50, (or 0.33, 0.00, 0.166, and 0.166), respectively. The determined g_J^{eff} factor of 0.5260±0.0006 and 0.1688±0.004, for the $J'=1$ and 2 levels of $I(|\Omega|=1)(v=0)$ state is compelling evidence that the dominant contribution to the $I(|\Omega|=1)(v=0)$ state is either a $^3\Pi_1$ state or, as originally suggested by Edvinsson and co-workers in 1967 [3], a $^1\Pi$ state.

As mentioned above, there is no calculated |Ω|=1 state having a dominant $^1\Pi$ character in the energy range of the observed $I(|\Omega|=1)(v=0)$ state. The most extensive prediction of the ThO excited states can be found in the dissertation by Tyagi [12]. That calculation predicted an |Ω|=1 state at 20221 cm^{-1}, but the predicted composition of this state is predominately $^3\Sigma^+$ (71%) in nature and with only 5% $^1\Pi$ character. As established above, the g_J^{eff} factors for such a state are expected to be much larger than the

observed values. This same excited state was predicted by Küchle et al. [7] to have an energy of 19040 cm^{-1} and a 76% $^3\Sigma^+$, 18.6% $^1\Pi$, and 2.1% $^3\Pi$ composition. This predicted state was assigned to the experimentally observed $D(|\Omega|=1)$, which has a T_0 of 15946 cm^{-1}.

An $|\Omega|=1$ state with predominant $^3\Pi$ character arising from the $Th^{2+}(7s5p)O^{2-}$ configuration is calculated at 21962 cm^{-1} [12]. The assignment of this predicted state to the observed $I(|\Omega|=1)(v=0)$ state is compatible with the observed g_J^{eff} values. Unfortunately, this assignment is not consistent with the observed trend in $|\vec{\mu}_{el}|$ of $(X^1\Sigma^+)$ < $|\vec{\mu}_{el}|(E(\Omega=0^+))$ < $|\vec{\mu}_{el}|(I(|\Omega|=1))$. A state with a dominant $Th^{2+}(7s5p)O^{2-}$ configuration would be expected to have a $|\vec{\mu}_{el}|$ value only slightly larger than that of $X^1\Sigma^+$ state because the 5*p* orbital is nearly as highly polarizable as with the 7*s* orbital. It seems more likely that the $I(|\Omega|=1)(v=0)$ state has a dominant $Th^{2+}(7s5f)O^{2-}$ configuration, as predicted by ligand field theory [9].

VI. SUMMARY

The magnetic and electric tuning and the field-free energies of the low-*J* branch features of the $I(|\Omega|=1)-X^1\Sigma^+(0,0)$ band of ThO, have been characterized. This information, combined with the previously determined properties of the $H^3\Delta_1$ state [13], will facilitate planned eEDM experiments. Furthermore, the determined bond lengths, g-factors and $|\vec{\mu}_{el}|$ will serve as benchmarks for the various computational methodologies to be used to predict the excited states of ThO.

Table I. The observed field-free transitions wavenumber (cm^{-1}) for the $I(|\Omega| = 1) - X\,^1\Sigma^+(0,0)$ band of ThO.

Line	Observed	Dif. [a] $\times 10^{-4}$	Line	Observed	Dif. [a] $\times 10^{-4}$
$P(2)$	19 537.7213	5	$Q(5)$	19 538.9329	7
$P(3)$	19 537.0471	3	$Q(6)$	19 538.884	3
$P(4)$	19 536.3678	0	$Q(7)$	19 538.8274	4
$R(0)$	19 539.7127	1	$Q(8)$	19 538.7625	2
$R(1)$	19 540.3666	1	$Q(9)$	19 538.6896	2
$R(2)$	19 541.0151	-3	$Q(10)$	19 538.6083	-2
$Q(1)$	19 539.0449	-6	$Q(11)$	19 538.5196	1
$Q(2)$	19 539.0293	-1	$Q(12)$	19 538.4228	4
$Q(3)$	19 539.005	-1	$Q(13)$	19 538.3169	-3
$Q(4)$	19 538.9712	-15	$Q(14)$	19 538.2036	-3
Std. dev.=0.0005 cm^{-1}					

a) Observed-calculated, obtained using optimized parameters.

Table II. The observed Stark shifts (MHz) .

Line	Field[a]	Obs.	Dif. [b]	Line	Field[a]	Obs.	Dif. [b]
R(0)	2222 ⊥	-2315	-2	*P*(2)	1111 ||	-1205	28
	2222 ⊥	2339	-2		1111 ||	1114	17
	1666 ⊥	-1738	20		556 ||	-630	5
	1666 ⊥	1724	-10		556 ||	528	-6
	1389 ⊥	-1477	1				
	1389 ⊥	1448	14	*Q*(1)	444 ||	-430	-4
	1111 ⊥	-1230	-35		444 ||	511	2
	1111 ⊥	1139	4		222 ||	-192	1
	556 ⊥	-628	-2		222 ||	272	-9
	556 ⊥	550	7		111 ||	-71	9
	278 ⊥	-362	-23		111 ||	176	6
	278 ⊥	274	23		56 ||	-36	-7
	139 ⊥	-205	-8		56 ||	111	-8
	139 ⊥	100	-8				
	69 ⊥	-143	-13	*Q*(1)	782 ⊥	848	-5
	69 ⊥	29	-11		669 ⊥	728	-10
					556 ⊥	622	-1
P(2)	1111 ⊥	-1230	-4		278 ⊥	-236	16
	1111 ⊥	1126	21		278 ⊥	335	-3
	833 ⊥	-919	9		222 ⊥	-195	-2
	833 ⊥	829	8		222 ⊥	273	-8
	556 ⊥	-630	3		111 ⊥	-73	7
	556⊥	524	-11		111 ⊥	163	-6
	389 ⊥	-452	5		56 ⊥	-8	21
	389 ⊥	348	-15		56 ⊥	111	-8
	278 ⊥	-348	-7				
	278 ⊥	244	-5		Std. Dev.= 12		

[a] The field strength (V/cm) and orientation: ⊥ =perpendicular, ||=parallel.
[b] Observed-calculated, obtained using optimized parameters.

Table III. The observed Zeeman shifts and splitting (MHz) at 3163 Gauss.

Line, pol. [a]	$\lvert M'_J \rvert$	Splitting	
		Obs. [b]	Dif. [c]
$R(0)$, ⊥	1	4646	-9
$P(2)$, ⊥	1	4654	-1
$P(2)$, ||	1	4663	8
$Q(1)$, ||	1	4650	-5
$Q(1)$, ⊥	1	4660	5
$Q(2)$, ||	2	2948	39
	1	1516	-24

[a] Orientation: ⊥ =perpendicular, ||=parallel.

[b] Observed splitting between features having the indicated values of $\lvert M_J \rvert$.

[c] Observed-calculated splitting obtained using optimized g_J^{eff} values for the $J' = 1$ and 2 levels of 0.5260±0.0006 and 0.1688±0.004, respectively.

Acknowledgement

This research has been supported by the National Science Foundation, Division of Chemistry, CHE-1265885 (ASU) and Physics (Grant PHY-0758045).

Figure Captions

Figure 1. The laser excitation spectrum near the origin of the $I(|\Omega| = 1) - X\,^1\Sigma^+(0,0)$ band of ThO. The spectrum is a collection of numerous 7 GHz scans and is not corrected for variation in production and/or laser power variation.

Figure 2. The $R(0)$ (19 539.7127 cm^{-1}) line recorded field free and in the presence of 278 V/cm static electric field with perpendicular polarization ($\Delta M_J = \pm 1$) and associated energy levels.

Figure 3. The $R(0)$ (19 539.7127 cm^{-1}) and $Q(1)$ (19 539.0449 cm^{-1}) lines recorded field free and in the presence of 3163 G static magnetic field with nominal perpendicular polarization ($\Delta M_J = \pm 1$) and associated energy levels. The weak feature in the middle of the Zeeman spectra is the $\Delta M_J = \pm 0$ transitions resulting from imperfect field alignment.

Reference

1. J. Baron, W. C. Campbell, D. DeMille, J. M. Doyle, G. Gabrielse, Y. V. Gurevich, P. W. Hess, N. R. Hutzler, E. Kirilov, I. Kozyryev, B. R. O'Leary, C. D. Panda, M. F. Parsons, M. F. Parsons, E. S. Petrik, B. Spaun, A. C. Vutha, and A. D. West, Science, **343**, 269 (2014).
2. D. L. Kokkin, T. C. Steimle, and D. DeMille, Phys. Rev. A, **90**, 062503 (2014)
3. G. Edvinsson, A. von Bornstedt, and P. Nylén, Arkiv Fysik, **38**, 193 (1967).
4. C.T. Dewberry, K.C. Etchison, and S.A. Cooke, Phys. Chem. Chem. Phys., **9**, 4895 (2007).
5. F. Wang, A. Le, T. C. Steimle, and M. C. Heaven, J. Chem. Phys., **134**, 031102 (2011).
6. A. A. Buchanachenko, J. Chem. Phys., **133**, 041102 (2010).
7. W. Küchle, M. Dolg, H. Stoll, and H. Preuss, J. Chem. Phys., **100**, 7535 (1994).
8. J. Paulovič, T. Nakajima, K. Hirao, R. Lindh, and P.A. Malmqvist, J. Chem. Phys., **119**, 798 (2003).
9. V. Goncharov, J. Han, L. A. Kaledin, and M. C. Heaven, J. Chem. Phys., **122**, 204311/1 (2005).
10. N. Beverini,E. Maccioni, and F. Strumia, J. Opt. Soc. Am., **15**, 2206 (1998).
11. H. Knöckel, B. Bodermann, and E. Tiemann, Eur. Phys. J. D, **28**, 199 (2004).
12. R. Taygi, Ph.D. Thesis, Ab Initio Studies of Systems Containing Actinides using Relativistic Effective Core Potentials, The Ohio State University, 2005.

13. A. C. Vutha, B. Spaun, Y. V. Gurevich, N. R. Hutzler, E. Kirilov, J. M. Doyle, G. Gabrielse, and D. DeMille, Phys. Rev. A, **84**, 034502 (2011).

Figure 1

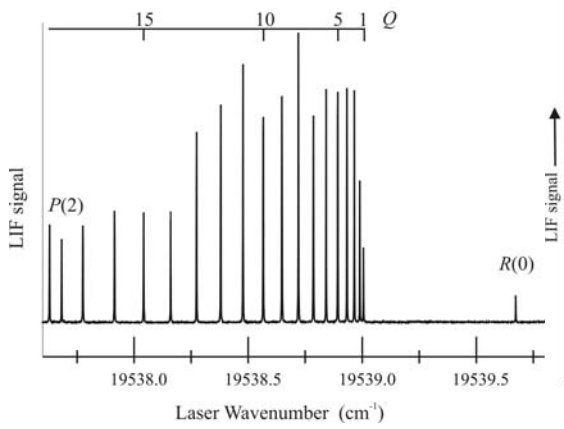

Figure 2

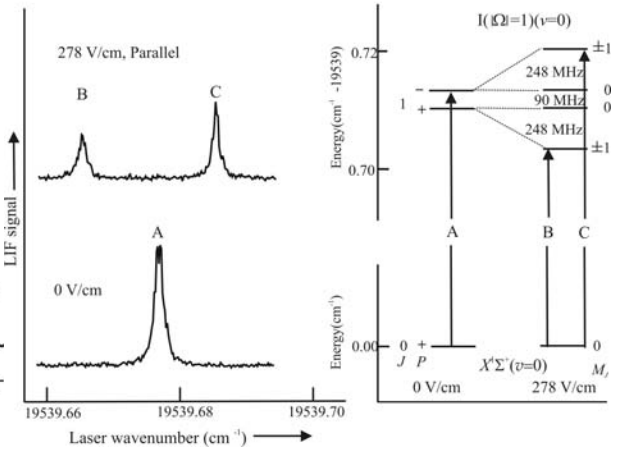

Figure 3